Optics and Laser Technology 109 (2019) 149–156

Contents lists available at ScienceDirect

Optics and Laser Technology

journal homepage: www.elsevier.com/locate/optlastec

Full length article

Raman and time-resolved pulsed photoacoustic spectroscopy of solid trinitrotoluene in graphite mixture: For identification of double resonant optical phonon signatures

K.S. Rao[a,b], A.K. Chaudhary[a,*]

[a] Advanced Center for Research in High Energy Materials (ACRHEM), University of Hyderabad, 500046, India
[b] The Guo China-US Photonics Laboratory, Changchun Institute of Optics, Fine Mechanics and Physics, Chinese Academy of Sciences, Changchun, China

HIGHLIGHTS

- Graphite as a sensor for identification of TNT using 1064 nm wavelength.
- The PA study with respect to different weight percentage of graphite in TNT matrix.
- Identification of acoustic and optical phonons waves transfer mechanism between GP and TNT using 785 nm wavelength.
- Development of a new tool for detection and identification of explosive molecules using commercially available laser systems.

ARTICLE INFO

Keywords:
Raman spectra
Trinitrotoluene
Graphite
Photoacoustic spectrum

ABSTRACT

The optical phonon waves transfer mechanism between pure graphite (GP) and trinitrotoluene (TNT) using 1064 nm as an excitation wavelength based on the double resonant Raman effect and the pulsed photoacoustic (PA) technique has been investigated. The study was carried out at a different weight percentage of GP within TNT with respect to the two excitation wavelengths of 532 nm and 1064 nm (30 ps, 10 Hz, Q-switched Nd: YAG laser). The equal and double proportional matrix of the GP and TNT (solid samples) generate a strong PA signal with high quality factor (Q-factor) due to the interaction of optical phonons of GP and TNT in the same phase. The Raman spectra, recorded at 785 nm wavelength provides an insight on the pi-electron coupling between the GP and TNT. The obtained experimental results confirm that the pure GP and its derivatives, which have a SP^2/SP^3 hybridization, can be used to develop a new sensing optode for the detection and identification of explosive molecules in the visible and near-IR wavelengths range.

1. Introduction

The detection of solid high energy materials (HEMs) or explosives in visible and NIR region using photoacoustic (PA) spectroscopy is still a challenging task due to the absence of absorption bands in this region. Many optical and chemical analytical techniques for the detection of explosives are reported by different groups [1–6]. These analytical techniques were demonstrated on the basis of the absorption or emission of incident radiation from the analysts. Among all, PA spectroscopy is one of the most versatile and potent absorption-based technique because it can identify molecules in the solid, liquid, and gaseous phase in trace level using deep UV, IR, and THz radiation [7–16]. High power pulsed and CW lasers of 532 nm and 1064 nm wavelengths are easily available, therefore, several researchers have demonstrated the wide range of applications in the field of laser spectroscopy for different materials at these wavelengths [17–23]. In present report, we have demonstrated the new mechanism of detection of the explosive using graphite (GP) as a sensing medium at 532 and 1064 nm wavelength range.

Recently, Sharkaway et al. have reported the laser-induced PA spectroscopy for trace detection of explosives using 1064 nm obtained from Nd: YAG laser, which is used in a combination of optical interferometry technique [17]. However, the strength of the generated acoustic signals was quite low. Similarly, TNT is detected by Haibo Zhou et al. using ultra-high Raman scattering of off-resonated p-amino benzenethiol (PABT) through the formation of TNT-PABT complex, where silver nanotubes arrays were used for enhancing the Raman signal [18]. On the other hand, a double resonant Raman spectroscopy

* Corresponding author.
E-mail addresses: akcphys@gmail.com, anilphys@yahoo.com (A.K. Chaudhary).

https://doi.org/10.1016/j.optlastec.2018.08.001
Received 11 January 2018; Received in revised form 20 July 2018; Accepted 2 August 2018
Available online 07 August 2018
0030-3992/

is one of the attractive technique, which is widely used to investigate the disorder and defects in the graphite-based system [19]. In addition, the detection and characterization of TNT using different optical techniques have been reported [16,20–23]. Mcnesby et al. have reported the Raman spectra of TNT and some other high-energetic materials using Fourier transform Raman (FTR) spectroscopy by employing near-IR laser radiation with a scattering source of 1060 nm [20]. M. Snels et al. have detected the solid explosive TNT in the near infrared spectral range between 1560 nm and 1680 nm using CW cavity ring down (CRD) spectroscopy [16]. Pushkarsky et al. demonstrated the detection of TNT using laser-based photoacoustic technique [21]. They have explored continuous-wave high-power quantum cascade laser in external grating cavity geometry tunable up to 400 nm and extended up to 7300 nm. They have also used the flash heater to evaporate solid TNT in a CRD absorption cell. Deshmukh et al. have investigated the TNT in water samples collected from nearby military training center using solid phase microextraction technique coupled with Fourier transform Raman spectroscopy [22]. Idros et al. demonstrated the colorimetric-based detection of TNT explosives using functionalized silica nanoparticles [23].

In our previous report the promising use of 532 nm wavelength to identify the TNT in GP mixture using pulsed PA technique combined with double resonant Raman effect has been reported [24]. In the present study, we have introduced the use of fundamental wavelength (i.e. 1064 nm) of Nd: YAG laser system of pulse duration of 30 ps and 10 Hz repetition rate for recording of characteristic PA spectra of TNT in different weight percentage of GP. In addition, the Raman spectra of GP, TNT, and GP + TNT at 785 nm wavelength have been recorded. The generation of PA signal from TNT in GP matrix is going to open a new channel of research in explosive detection.

Pure GP does not emit any light photons because there is no transition between the conduction and valence energy bands. But it strongly emits thermal radiation, which falls in the far infrared region. Therefore, source medium GP plays an important role in interaction with the carbon in C—H—O group of TNT molecules. In the case of TNT, two energy bands (Raman bands) are generated due to NO_2 and cyclic aromatic ring, while for GP it is attributed to D-band. The carbon atoms of GP are arranged in a hexagonal structure, where one carbon atom forms a covalent bond with three surrounding atoms [25]. It is well-known that carbon has valence of 4 and it can make four bonds. In the case of GP three electrons of carbon form three bonds among themselves, and the other free electron floats freely between two layers of carbon plates as shown in Fig. 1(a). This free electron is delocalized and mobile by nature. Thus, it can conduct the electricity and give the GP the property of an electric conductor despite being a non-metal. A force created between these two layers of carbon with the aid of the electrons is known as Van Der Waal force [26,27]. Graphene is a two-dimensional (2D) building block for carbon allotropes of every other dimensionality.

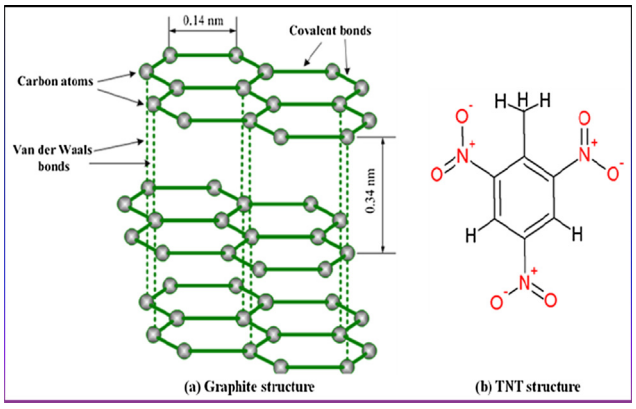

Fig. 1. The structure of (a) graphite and (b) trinitrotoluene (TNT).

It can be stacked into 3D graphite, rolled into 1D nanotube, or wrapped into 0D fullerenes. The G and 2D Raman peaks change their shape, position, and relative intensity with respect to the number of graphene layers. Also, it reflects the evolution of the electronic structure and electron-phonon interactions. The origin of the D and G bands along with second-order D peak of graphene has been studied in [28].

The broad range of excitation energy of GP lies between 1.91 eV (649 nm) and 2.52 eV (488 nm) that shows the first and second-order Raman spectra of the GP respectively [28–33]. Raman spectroscopy is a well-established tool for vibration spectroscopic analysis and is employed for the identification and detection of explosives [20,34–37]. Wang et al. [29] have analyzed the Raman spectra of industrial TNT dissolved in acetone and reported seven major bands. They have used 1064 nm wavelength obtained from the diode-pumped Nd: YVO_4 solid laser as an excitation source. The 2D GP structure consists of two carbon atoms per unit cell, which are associated with six numbers of phonon modes. Among them, three belong to acoustic (A), and the other three to optic (O) phonon modes. The optic phonon modes are further divided into out of plane (OT) phonon mode, one longitudinal (L), and the other one transverse (iTO) [19].

The optical/acoustic phonons are responsible for transferring the vibrational energy and momentum from GP to TNT. This phenomenon was also perceived in the Raman spectra of samples. In this case, the shift in D and G bands of GP, as well as TNT bands in the GP + TNT mixture was observed. This is the indication of coupling of pi-electrons between GP and TNT (due to electron-phonon or phonon-phonon interactions) that leads to transfer the phonon waves momentum from GP to TNT. As a result, TNT can absorb the incident radiation that leads to generation of strong PA signal. The present study revealed that near-IR wavelengths could also be useful to identify solid TNT and other HEMs in the presence of GP using pulsed PA spectroscopy.

2. Experimental arrangements

The experiment was performed in three steps. In the first step, the mixture of TNT and GP were prepared in different weight proportions. The powder samples were converted into a circular disk of variable thickness in the form of pellets using two tons of pressure. In the second step, the mixture was placed in an aluminum cubic shaped PA cell of length 5 cm, width 5 cm, and height 6 cm. The fundamental and the second harmonic wavelengths, i.e. 1064 nm and 532 nm, obtained from Q-switched Nd: YAG laser of 30 ps duration at 10 Hz (PL-2250 Ekspla, Lithuania) were employed to excite the mixture of TNT and GP. The generated PA signal was recorded using a pre-polarized microphone (BSW, China), which was housed in a teflon (PTFE) jacket and placed at a distance of 1.0 cm from the sample cavity. The distance between the center of the sample and the microphone head was 2.2 cm. An aluminum plate had a window of one-inch diameter glass/quartz covered with a neoprene washer, which was used to cover the cavity. The generated PA signal was amplified using a preamplifier and fed to the digital storage oscilloscope (Tektronix, 200 MHz) for the recording of the time domain signal. The oscilloscope was connected to the personal computer, which has a data acquisition program developed using LabView software. In the third step pure TNT & GP and their mixtures were subjected to portable Raman spectrometer, λ = 785 nm (B &W Tek, USA) for the recording of Raman spectra.

3. Results and discussion

3.1. 1064 nm based photoacoustic spectra of TNT with GP

Fig. 2(a and b) shows the PA spectra of a pure GP (2 mg) and composite (GP + TNT, 1:1 ratio by weight) respectively. The PA spectra are recorded at data acquisition time t = 1 ms and at incident laser energy E_{in} = 2.0 mJ. The excited acoustic modes for the matrix of GP and TNT (GP + TNT) show the shift in the frequency with respect to the

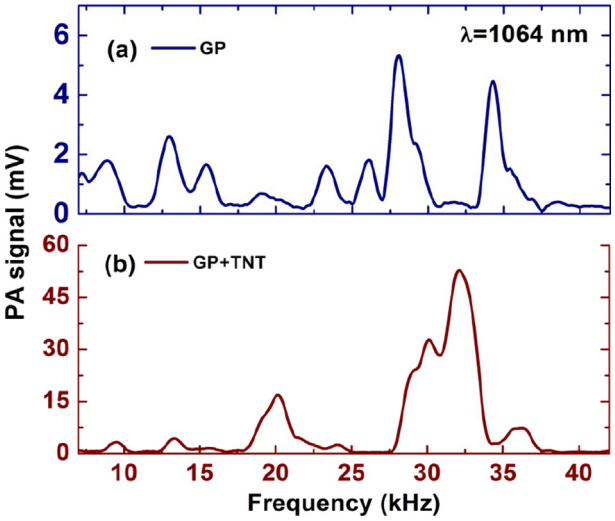

Fig. 2. PA spectra of (a) GP (b) GP + TNT at 2.0 mJ and t = 1 ms.

pure GP frequency. For the GP + TNT the acoustic modes show a pair of peaks, a broad profile between 28 and 35 kHz, and have one of the strongest modes at 32.0 kHz. In addition, two acoustic modes located at 28.1 and 34.3 kHz of pure GP spectrum are merged in the PA spectra of GP + TNT mixture. Also, it shows the broadband profile with ten times higher intensity. All other acoustic modes of pure GP also show a shift in their frequencies in GP + TNT mixture. It confirms the process of exchange of the optical phonons momentum between GP and TNT which is explained using the double resonant Raman effect.

Fig. 3 shows the PA spectra of GP and GP + TNT at t = 1 ms between 0.5 and 3.0 mJ energy range. The excited acoustic modes for pure GP and a mixture of GP + TNT are shown in Table 1. It is clearly observed that the order of excited acoustic modes and their corresponding frequencies remain unchanged with respect to variation of the incident laser energy. The molecules of pure TNT (solid) provide the intensity of PA signal of an order of 1.8 mV at E_{in} = 3.0 mJ and t = 1 ms, whereas pure GP shows negligible enhancement in the PA signal intensity at 0.5 mJ. However, the mixture of TNT and GP shows a significant rise in PA signal intensity. This confirms the coupling of pi-electrons/phonons of TNT and GP excited by 1064 nm wavelength radiation. Consequently, highest strength of PA signal is generated for GP + TNT. Also, it is clearly observed that there are less excited acoustic modes of GP + TNT than of the pure GP. However, all other mixtures show strong PA spectra with a small shift in their corresponding acoustic modes.

Table 1
Excited acoustic modes of GP and GP + TNT and their corresponding intensities at 1064 nm.

GP	kHz:	8.9	12.9	15.4	19.0	23.3	26.1	28.1	34.3
	mV:	1.79	2.59	1.66	0.08	1.61	1.81	5.32	4.46
GP + TNT	kHz:	9.6	13.3	20.1	30.1	32	36.1		
	mV:	3.22	4.33	16.86	32.78	52.56	7.28		

Table 2
Initial weights and the corresponding weight percentage of GP and TNT.

Matrix	Initial weight		Percentage	
	GP (mg)	TNT (mg)	GP (%)	TNT (%)
1	1	2	33.3	66.6
2	2	2	50.0	50.0
3	3	2	60.0	40.0
4	4	2	66.6	33.3
5	5	2	71.4	28.6

3.2. PA spectra of different weights percentage of GP + TNT

For verification of the optical phonon momentum exchange in GP and TNT we have repeated the experiment with a different weight percentage of GP in TNT. A mixture of TNT and GP was prepared using the initial weight of 2.0 mg of TNT. Later on, the quantity of GP varied from 1.0 to 5.0 mg in the TNT composition. The initial weight and its equivalent percentage of GP and TNT are listed in Table 2.

Fig. 4 shows the PA spectra of TNT mixed in GP in different weight proportions at t = 1 ms, E_{in} = 3.0 mJ, in the range between 7 and 40 kHz for the excitation wavelengths of 1064 nm and 532 nm respectively. It confirms that the pair of acoustic peaks for a different weight percentage of GP possess different intensities. In case of 1064 nm-based PA spectra of GP + TNT mixtures, the acoustic modes of 29 kHz and 32 kHz possess the double resonant nature, whereas, the mode near to 20 Hz shows a single broad peak for matrix-1, 2, and 3, respectively. However, on further increase of the GP quantity, i.e. for matrix-4 and -5, the modes at 29 kHz and 32 kHz merged together and this shows the broadening effect. At matrix-4 the 32.5 kHz mode is much broader than the other compositions. However, 20 kHz mode slightly shifted to 22.5 kHz and split in two peaks possessing the double resonant nature (see Fig. 4(a)). In addition, for the matrices-4 and 5, the low order acoustic modes lying between 8 and 14 kHz are excited with similar intensity. In the case of 532 nm at matrix-3 the acoustic modes at 17.3 and 28.8 kHz have the similar intensities. In this case the strongest acoustic mode is located at 29 ± 0.3 kHz, except the peak matrix-5,

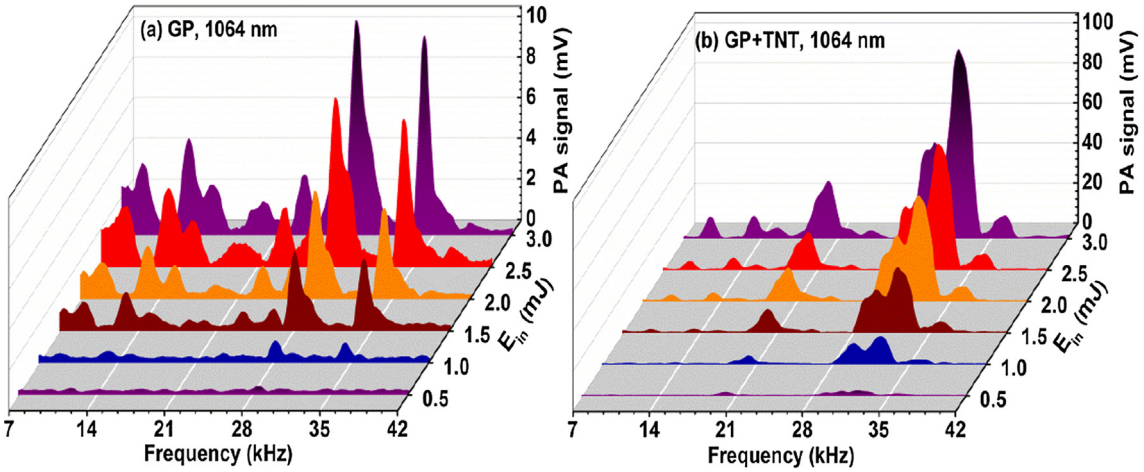

Fig.3. PA spectra of (a) GP (b) GP + TNT for 1064 nm.

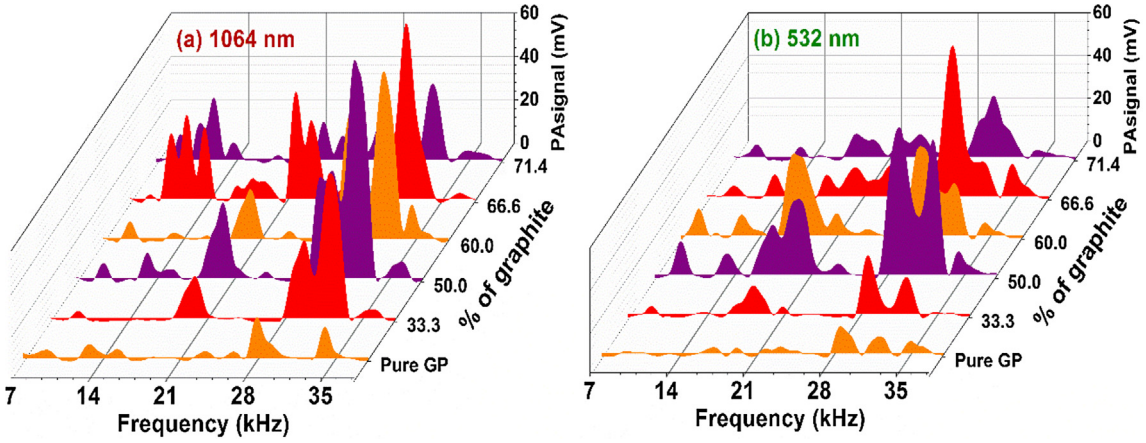

Fig. 4. PA spectra of a mixture of TNT and graphite (GP) at different weight percentage for (a) 1064 nm and (b) 532 nm at E_{in} = 3.0 mJ and t = 1 ms.

which is located at 30 kHz. The PA spectra for the matrix-4 and -5, the acoustic modes 29 and 32 kHz are also merged together.

The PA spectra of pure GP show the presence of three peaks at 28.7, 32.3, and 35.2 kHz respectively. These peaks are gradually turned into a single predominant peak for both wavelengths of 1064 nm and 532 nm. Particularly, the matrix-5 has single mode at 32.5 (1064 nm) and 29.3 kHz (532 nm) respectively. The PA results reveal that in higher quantity of GP the mixture shows a broadening effect in the higher order acoustic modes and shift in the lower order acoustic mode. Moreover, the strength of the pure GP signal is comparatively lower than the signal of mixture of GP + TNT for both excitation wavelengths. The PA signals of GP and TNT at 1:1 (matrix-2) and 2:1 (matrix-4) ratios are stronger than the other matrices (see Fig. 4). It might be attributed to the phonon waves are in the same phase, which lead to enhancing the double resonance Raman signal of the composition. However, for other mixtures there is a phase mismatch between the phonon waves, which leads to lower intensities of PA signal. The strength of PA signal and the corresponding acoustic frequencies of different matrices reveal the signature of TNT in GP.

3.3. The behavior of acoustic modes with respect to different weights of graphite

Acoustic modes' behavior and the corresponding strength of PA signal vary with the concentration of GP in TNT. Fig. 5(a and b) depicts the behavior of ~30 kHz mode of different mixtures using incident laser energy from 0.5 to 3.0 mJ respectively. The intensity of PA signal increases with respect to the energy of the incident laser. For all the incident laser energies it is noticed that the behavior of acoustic modes is similar for the different compositions of GP + TNT. Fig. 5 confirms that the strength of PA signal is high for matrices-2 and 4, and is low for matrices-1, -3, and -5.

3.4. The responsivity of PA cell with respect to incident laser energy

Fig. 6(a and c) shows the linear increment of the intensity of PA signal with respect to the incident laser energy for various matrices at t = 1.0 ms. The slope of the linear fit of corresponding data points (before the saturation limit) of PA signal provides the responsivity of PA cell with respect to the incident laser energy.

Fig. 6(a and b) shows the responsivity curve of PA cell at different concentrations of GP. The value of responsivity of pure GP is lower than the values for different mixtures that indicates an exchange of optical phonons between TNT and GP excited with 532 nm and 1064 nm. The change in the responsivity of GP + TNT is a clear sign of morphological change. The responsivity of the sample follows the nonlinear growth with increasing percentage of the GP. The responsivity is linearly increased for even proportions of GP (matrices-2 and -4), while for the odd mass concentration of GP (matrices-3 and -5), the responsivity shows saturation behavior [see Fig. 6(b and d)]. GP has much stronger absorption than pure TNT at 532 nm and 1064 nm, therefore, PA signal curves show the linear growth in Fig. 6(a and c). However, the responsivity does not follow the linear behavior for the different GP + TNT matrices. Fig. 6(b and d) shows that the highest responsivity is achieved for the matrix-2 and 4 due to the generation of high PA signal with respect to incident laser energy. It is inferred that the excited optical phonons waves of GP are in the same phase with phonon waves of TNT for the equal and double quantity of GP. In this case the phonon waves are interacting constructively and superimposed on each other. As a result, strong phonon waves are generated, which are measured in

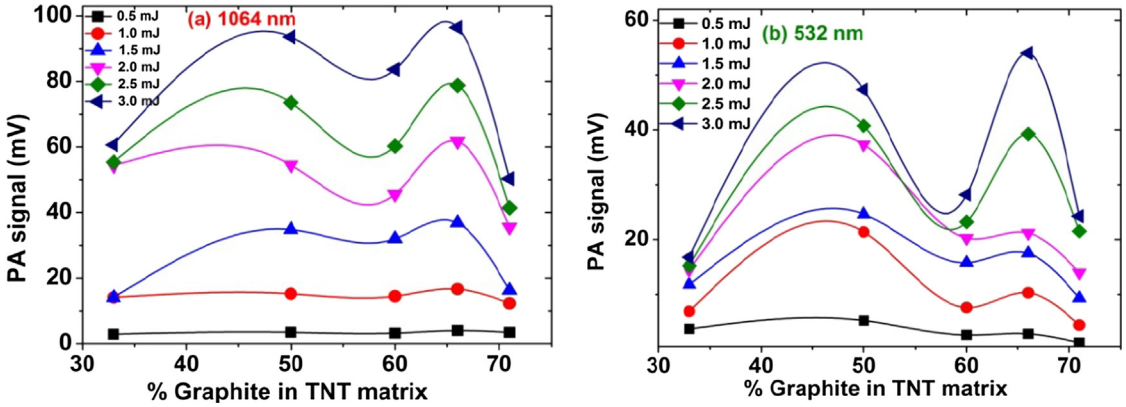

Fig. 5. The behavior of one of the predominant acoustic mode (~30 kHz) w.r.to different weight percentage of graphite in TNT for (a) 1064 nm and (b) 532 nm.

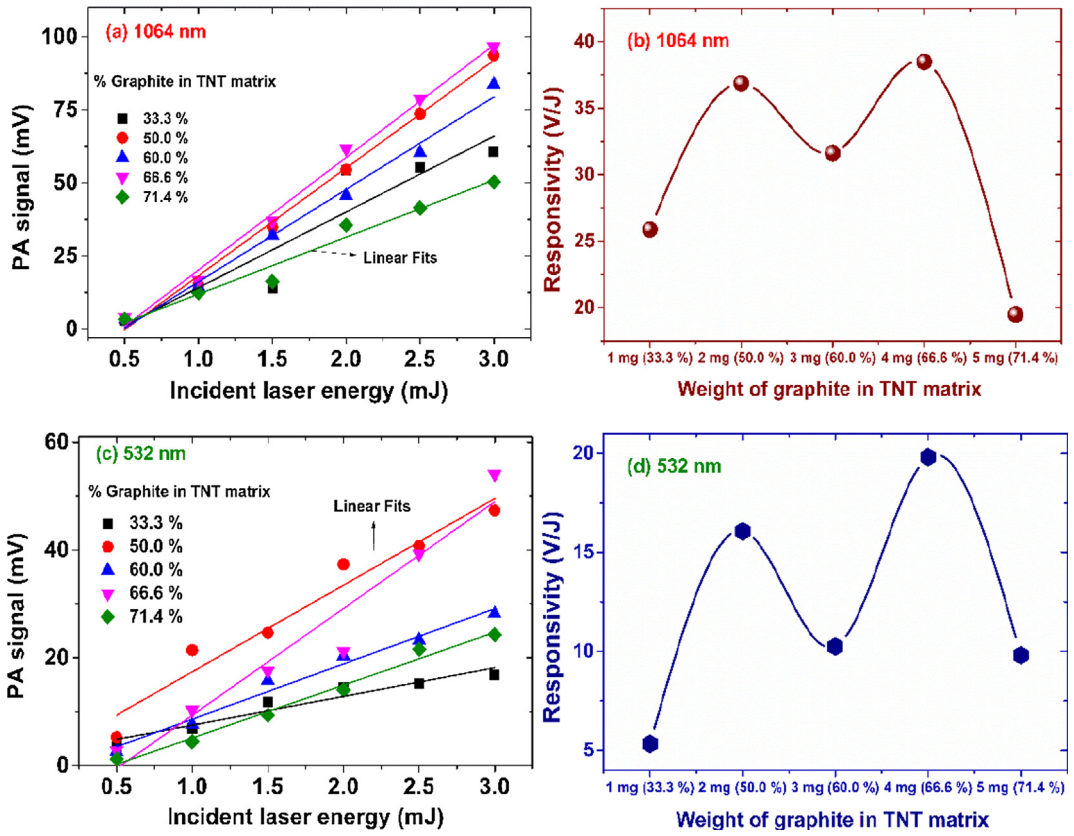

Fig. 6. Linear fits of PA signal and its responsivity for different weight percentage of graphite in TNT, for (a and b) 1064 nm and (c and d) 532 nm, respectively.

terms of acoustic signals. However, for the odd mixtures, i.e. -1,-3, and -5, the optical phonon waves have phase lag, which is responsible for the destructive interference. Therefore, these matrices show weak PA signal.

3.5. Double resonance nature of acoustic modes and Q-factor of PA cavity

The Q-factor of the PA cavity is defined as the ratio of accumulated energy to that of energy loss per cycle. Physically, this parameter is given by the ratio of the central frequency (ω) to full width at half maxima (FWHM or Δω) of the corresponding acoustic mode, i.e.

$$Q = \frac{\omega}{\Delta\omega} \tag{1}$$

This equation shows that the highest Q-factor can be achieved either at high frequencies or with low FWHM. Fig. 7(a and b) shows the Lorentz fits of doubly resonant acoustic modes. i.e. 29 and 32 kHz corresponding to excitation wavelengths 1064 nm and 532 nm, respectively for different compositions of TNT and GP. Therefore, we have chosen these modes to find the quality factors of PA cavity. In addition, the intensities of acoustic modes reveal that the higher wavelength (1064 nm) is responsible for the generation of high orders of optical phonons, which help to excite the higher order acoustic modes, whereas lower wavelength (532 nm) excites the comparatively lower optical phonon modes. At 1064 nm the double resonant modes for different weights of TNT and GP lay between the individual modes of pure GP, which are present at 28 and 34.2 kHz [see Fig. 7(a)]. However, in the case of 532 nm the double resonance nature is high for mixture-2 (50–50% of GP and TNT) as shown in Fig. 7(b). It is interesting to note that the double resonance of acoustic modes decreases with increasing

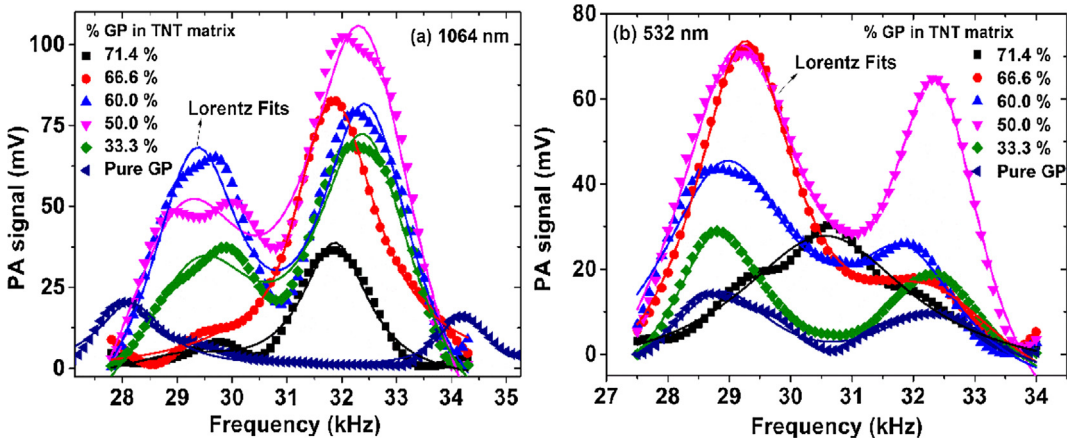

Fig. 7. Lorentz fits of double resonant acoustic modes for (a) 1064 nm (b) 532 nm w.r.to different weight proportions of TNT and GP.

Table 3
Quality factors of PA cavity.

% GP in TNT	Q for 1064 nm		Q for 532 nm	
	~29 kHz	~32 kHz	~29 kHz	~32 kHz
33.3% (1 mg)	10	15	15	14
50.0% (2 mg)	9	12	11	18
60.0% (3 mg)	14	15	11	14
66.6% (4 mg)	25	17	15	11
71.4% (5 mg)	11	21	9	–
Pure GP (2 mg)	19	34	13	12

quantity of the GP. In the case of matrix-5 the double resonant response is very weak, whereas the 29 kHz and 32 kHz peaks are overlapped and broaden their frequency range that lays between 28 and 34 kHz, and the central frequency is shifted to 30.24 kHz range.

The values of Q-factor of PA cavity at double resonant acoustic modes at 29 and 32 kHz are comprised in Table 3. In case of 1064 nm, the Q-factors for matrix-4 are of 25 and 17 at 29 kHz and 32 kHz, respectively, which are higher than the other mixtures. However, for 532 nm the Q-factor value of matrix-4 is 15 at 29 kHz. Whereas, the matrix-2 has the highest Q-factor of 18 at 32 kHz.

The PA results obtained from above sections based on the effect of incident laser energy, the value of Q-factors of PA cell with different weight percentage of GP confirm that the TNT molecules have better interaction with 1064 nm and 532 nm radiation. Our experimental findings based on PA spectroscopy are supported by Raman spectra. The shift in the wave numbers of the mixture of TNT and GP indicates the pi-electron coupling, which leads to transfer of phonon momentum at different weights of GP.

3.6. Raman spectra of TNT with GP at 785 nm

In our previous report [24] we have recorded 532 nm-based Raman spectra of pure GP, TNT, and GP + TNT. The spectra helped us to identify the role of G-band of GP in solid TNT lines, which was downshifted (redshift) by 4 cm^{-1}. The experimental findings established the role of electrons/phonon transfer mechanism between GP and TNT due to an interaction of pi-orbitals. The present study highlights the effect of 785 nm for the recording of Raman spectra of TNT and GP and their mixtures. The spectral lines show either red or blue shift of the order of 4 cm^{-1}. For example, the strongest Raman line of TNT present at 1364.27 cm^{-1} is downshifted to 1352.44 cm^{-1}. Whereas, the G band of GP present at 1578.29 cm^{-1} is downshifted to 1576.57 cm^{-1}. Fig. 8(a) shows the Raman spectra of pure GP, TNT, and GP + TNT. Fig. 8(b and c) clearly shows the red/blue shift of pure samples in their corresponding mixture. The *'D'* band of GP (1314.51 cm^{-1}) and TNT (1364.27 cm^{-1}) coincide at 1352.44 cm^{-1} in the case of GP + TNT. The shift in the wavenumbers confirms the role of the incident photon for excitation of electrons, which initiates the phonon wave exchange mechanism efficiently between GP and TNT at 785 nm. The spectra posses well resolved Raman lines with a strong

Table 4
Raman Lines shift of pure GP with respect to GP + TNT mixture.

Raman lines (cm^{-1})			Band description
Graphite	GP + TNT	Δν (GP)	
1314.51	–	–	D band
1578.29	1576.57	1.72	G band
2326.52	2328.25	−1.73	G* band
2645.47	2659.26	−13.79	2D band

Table 5
Raman lines' shift values for pure TNT [38].

Raman lines (cm^{-1})			Assignment
TNT	GP + TNT	Δν (TNT)	
268.51	280.09	−11.58	
325.45	319.74	5.71	Framework distortion mode
366.69	352.49	14.2	
639.65	631.79	7.86	
790.86	790.40	0.46	C–H out-of-plane bend
822.28	823.16	−0.88	nitro-groups Scissoring
938.14	935.22	2.92	
1087.39	1085.21	2.18	
1209.14	1205.90	3.24	C_6H_2–C vibration
1364.27	1352.44	11.83	NO_2 symmetric stretching vibration
1531.19	1543.81	−12.62	NO_2 asymmetric stretching vibration
1617.60	1616.22	1.38	C=C aromatic stretching vibration

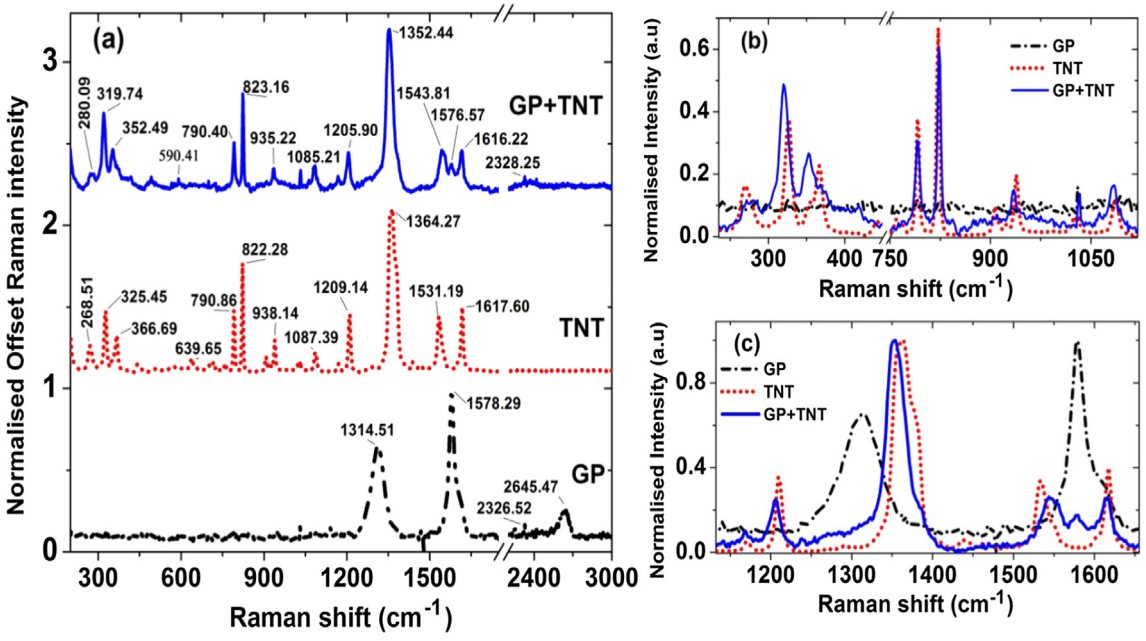

Fig.8. Raman spectra of TNT, GP, and mixture of TNT and GP.

shift between the wave numbers of 200–1800 cm^{-1}. However, some important bands between 2920 and 3160 cm^{-1} are not presented. The Raman lines of pure GP, pure TNT, GP + TNT and their corresponding shift values are comprised in Tables 4 and 5 respectively.

The G band position of GP shifts towards the higher wave number when it converts to nanocrystalline form, and the same shift even becomes lower when it transorms into the amorphous phase of carbon [39]. The G band peak at 1578.29 cm^{-1} with a small FWHM suggests that the GP has a well-ordered crystalline structure. However, the GP + TNT mixture shows the downshift (redshift) trends in G band position with the broadening effect, i.e. increase of FWHM, which clearly indicates that the mixture becomes more amorphous [40]. However, in the case of GP + TNT most of the Raman lines show the red shift. Some of the lines present at 268.51, 822.28, and 1531.19 cm^{-1} show the blue shift. It is well known that the Raman scattering is inelastic that means the energy or frequency of incident photons is not the same as the energy of the scattered photons.

The vibration frequency (ν_o) of the molecular transition is defined in terms of force constant (k) by the following equation:

$$\nu_o = \frac{1}{2\pi}\sqrt{\frac{k}{\mu}} \tag{2}$$

where $\mu = \frac{m_1 m_2}{m_1 + m_2}$ is reduced mass of the molecules, TNT and GP molecules are interacting with excitation radiation due to pi-electron coupling. Consequently, the value of force constant (k) is directly associated with the red and blue shifts. Therefore, the interaction of TNT and GP mixture lead to absorption of the incident wavelength. As a result, most of the Raman lines of TNT possess redshift. However, TNT lines at 822.28 cm^{-1} and 1531.19 cm^{-1} possess blueshifts (gain energy). The shift (red or blue) in the Raman lines confirms the morphological change of GP + TNT mixture, which directly illustrates the bonding between GP and TNT. The Raman lines' contributions are due to nitro-groups scission and NO_2 asymmetric stretching vibrations, respectively. The nitro-groups scission and NO_2 asymmetric stretching vibration lead to reductions in the bond length of molecules that resulted in an enhancement of vibration frequency.

Finally, the results of Raman spectra reveal that there is a coupling between GP and TNT in terms of optical phonons or pi-electrons when the mixture is excited by the visible to near-IR radiation.

4. Conclusions

We have successfully recorded the time resolved photoacoustic spectra of TNT with different quantity of graphite from 1 to 5 mg using 532 nm and 1064 nm pulses obtained from 30 ps Nd: YAG laser systems. The study is based on the behavior of acoustic modes with different proportions of graphite and the responsivity of PA cell with incident laser energy, which provides the optical energy and momentum transfer from graphite to TNT. In addition, the Raman spectra of GP + TNT mixtures and pure TNT molecules supported the optical phonon waves exchange mechanism terms of double resonance Raman spectra due to pi-electron coupling. Finally, the study highlights that graphite can be used as a sensor for identification of high energy materials with commercially available laser systems from visible to near IR.

Acknowledgments

The authors gratefully acknowledge D.R.D.O., Ministry of Defense, Govt. of India, for financial support under ACRHEM Phase III grants (ERIP/ER/1501138/M/01/319/D(R&D). Thanks to Dr. K.V. Rao, Ex. Director, ACRHEM, the University of Hyderabad for encouragement.

Appendix A. Supplementary material

Supplementary data associated with this article can be found, in the online version, at https://doi.org/10.1016/j.optlastec.2018.08.001.

References

[1] J.S. Caygill, F. Davis, S.P.J. Higson, Current trends in explosive detection techniques, Talanta 88 (2012) 14–29, https://doi.org/10.1016/j.talanta.2011.11.043.
[2] C.M. Wynn, S. Palmacci, R.R. Kunz, M. Rothschild, A novel method for remotely detecting trace explosives.
[3] E. Erçağ, A. Üzer, R. Apak, Selective spectrophotometric determination of TNT using a dicyclohexylamine-based colorimetric sensor, Talanta 78 (2009) 772–780, https://doi.org/10.1016/j.talanta.2008.12.042.
[4] J.L. Anderson, A.A. Cantu, A.W. Chow, P.S. Fussell, R.G. Nuzzo, J.E. Parmeter, G.S. Sayler, J.M. Shreeve, R.E. Slusher, M. Story, Existing and Potential Standoff Explosives Detection Techniques, National Academies Press, Washington DC, 2004.
[5] W.O. Rivera, Standoff Raman spectroscopy system for detection of explosives, chemical warfare ajents simulants and toxic industrial compounds, 2008.
[6] K. Hasue, S. Nakahara, J. Morimoto, T. Yamagami, Y. Okamoto, T. Miyakawa, N.D. Academy, Photoacoustic spectroscopy of some energetic materials, propellants, Explos. Pyrotech. 20 (1995) 187–191.
[7] A. Miklós, P. Hess, Z. Bozóki, Application of acoustic resonators in photoacoustic trace gas analysis and metrology, Rev. Sci. Instrum. 72 (2001) 1937–1955, https://doi.org/10.1063/1.1353198.
[8] A.K. Chaudhary, G.C. Bhar, S. Das, Low-limit photo-acoustic detection of solid RDX and TNT explosives with carbon dioxide laser, J. Appl. Spectrosc. 73 (2006) 123–129, https://doi.org/10.1007/s10812-006-0046-8.
[9] A. Rosencwaig, Photoacoustic spectroscopy of solids, Opt. Commun. 7 (1973) 305–308, https://doi.org/10.1016/0030-4018(73)90039-4.
[10] A.F. El-Sherif, H.S. Ayoub, Y.H. El-Sharkawy, W. Gomaa, H.H. Hassan, The design and implementation of photoacoustic based laser warning receiver for harsh environments, Opt. Laser Technol. 98 (2018) 385–396, https://doi.org/10.1016/j.optlastec.2017.06.030.
[11] I. Bayrakli, Y.K. Erdogan, Photo-acoustic sensor based on an inexpensive piezoelectric film transducer and an amplitude-stabilized single-mode external cavity diode laser for in vitro measurements of glucose concentration, Opt. Laser Technol. 102 (2018) 180–183, https://doi.org/10.1016/j.optlastec.2017.12.034.
[12] B.S. Goldschmidt, A.M. Rudy, C.A. Nowak, D.P. Macoubrie, J.A. Viator, H.K. Hunt, Characterization of MgF2 thin films using optical tunneling photoacoustic spectroscopy, Opt. Laser Technol. 73 (2015) 146–155, https://doi.org/10.1016/j.optlastec.2015.04.019.
[13] A.G. Demir, B. Previtali, N. Lecis, Development of laser dimpling strategies on TiN coatings for tribological applications with a highly energetic Q-switched fiber laser, Opt. Laser Technol. 54 (2013) 53–61, https://doi.org/10.1016/j.optlastec.2013.05.007.
[14] S. Wallin, A. Pettersson, H. Östmark, A. Hobro, Laser-based standoff detection of explosives: a critical review, Anal. Bioanal. Chem. 395 (2009) 259–274, https://doi.org/10.1007/s00216-009-2844-3.
[15] M.R. Leahy-Hoppa, M.J. Fitch, X. Zheng, L.M. Hayden, R. Osiander, Wideband terahertz spectroscopy of explosives, Chem. Phys. Lett. 434 (2007) 227–230, https://doi.org/10.1016/j.cplett.2006.12.015.
[16] M. Snels, T. Venezia, L. Belfiore, Detection and identification of TNT, 2,4-DNT and 2,6-DNT by near-infrared cavity ringdown spectroscopy, Chem. Phys. Lett. 489 (2010) 134–140, https://doi.org/10.1016/j.cplett.2010.02.065.
[17] Y.H. El-Sharkawy, S. Elbasuney, Novel laser induced photoacoustic spectroscopy for instantaneous trace detection of explosive materials, Forensic Sci. Int. 277 (2017) 215–222, https://doi.org/10.1016/j.forsciint.2017.06.005.
[18] H. Zhou, Z. Zhang, C. Jiang, G. Guan, K. Zhang, Q. Mei, R. Liu, S. Wang, Trinitrotoluene explosive lights up ultrahigh Raman scattering of nonresonant molecule on a top-closed silver nanotube array, Anal. Chem. 83 (2011) 6913–6917, https://doi.org/10.1021/ac201407z.
[19] M.A. Pimenta, G. Dresselhaus, M.S. Dresselhaus, L.G. Cançado, A. Jorio, R. Saito, Studying disorder in graphite-based systems by Raman spectroscopy, Phys. Chem. Chem. Phys. 9 (2007) 1276–1290, https://doi.org/10.1039/B613962K.
[20] K.L. Mcnesby, J.E. Wolfe, J.B. Morris, Fourier transform Raman spectroscopy of some energetic materials and propellant formulations, J. Raman Spectrosc. 25 (1994) 75–87.
[21] M.B. Pushkarsky, I.G. Dunayevskiy, M. Prasanna, A.G. Tsekoun, R. Go, C.K.N. Patel, High-sensitivity detection of TNT, Proc. Natl. Acad. Sci. USA 103 (2006) 19630–19634, https://doi.org/10.1073/pnas.0609789104.
[22] A.V. Deshmukh, A. Pandey, Detection of chemical signatures of 2,4,6-Trinitrotoluene (TNT) in water samples using automated Solid-Phase Micro-extraction (SPME) coupled to FT-Raman spectroscopy, Malaysian J. Forensic Sci. 4 (2013) 30–32.
[23] N. Idros, M. Ho, M. Pivnenko, M. Qasim, H. Xu, Z. Gu, D. Chu, Colorimetric-based detection of TNT explosives using functionalized silica nanoparticles, Sensors 15 (2015) 12891–12905, https://doi.org/10.3390/s150612891.
[24] K.S. Rao, A.K. Chaudhary, F. Yehya, Investigation of solid carbon blacks using pulsed photoacoustic and double resonant Raman spectroscopy for the identification of trinitro-toluene, Sens. Actuat. B Chem. 231 (2016) 830–836, https://doi.org/10.1016/j.snb.2016.03.052.
[25] Q.C. Campbell, Graphite: properties, occurrences and uses, 2013, <https://www.scopus.com/inward/record.uri?eid=2-s2.0-4892893723&partnerID=40&md5=1c24fd0355283d3010c51db4406a36d0>.
[26] Properties and characteristics of graphite, <https://www.entegris.com/resources/assets/-6205-7329-0513.pdf>, 2003, doi:10.1002/ejoc.201200111.
[27] A.-B. Djurišić, E.-H. Li, Optical properties of graphite, J. Appl. Phys. 85 (1999)

7404–7410, https://doi.org/10.1063/1.369370.
[28] A.C. Ferrari, Raman spectroscopy of graphene and graphite: disorder, electron-phonon coupling, doping and nonadiabatic effects, Solid State Commun. 143 (2007) 47–57, https://doi.org/10.1016/j.ssc.2007.03.052.
[29] X. Wang, S. Chang, J. Yang, J. Tan, H. Jia, H. Yin, X. Li, G. Peng, Detection of TNT in acetone using Raman spectroscopic signature, in: Proc. SPIE 6622, Int. Symp. Photoelectron. Detect. Imaging 2007 Laser, Ultraviolet, Terahertz Technol. 662219 (February 22, 2008), 2007, pp. 662218–662219. doi:10.1117/12.790827.
[30] R. Escribano, J.J. Sloan, N. Siddique, N. Sze, T. Dudev, Raman spectroscopy of carbon-containing particles, Vib. Spectrosc. 26 (2001) 179–186.
[31] J. Hodkiewicz, Characterizing carbon materials with Raman spectroscopy, Sci. Thermo Fish. Appl. Note 51901.
[32] M. Pimenta, Studying disorder in graphite-based systems by Raman spectroscopy, Phys. Chem. Chem. Phys. 9 (2007) 1276–1291, https://doi.org/10.1039/b613962k.
[33] C. Pantea, T.W. Zerda, Microstructure of carbon blacks determined by X-ray diffraction profile analysis, Carbon N. Y. 40 (2002) 929–937.
[34] N.F. Fell, J.A. Vanderho, R.A. Pesce-rodriguez, K.L. Mcnesby, Characterization of Raman spectral changes in energetic materials and propellants during heating, J. Raman Spectrosc. 29 (1998) 165–172.
[35] K.L. Fell, N.F. Widder, J.M. Medlin, S.V. Morris, J.B. Pesce-Rodriguez, R.A. McNesby, Fourier transformraman spectroscopy of some energetic materials and propellant formulations. II, J. Raman Spectrosc. 27 (1996) 97–104.
[36] L. Nagli, M. Gaft, Y. Fleger, M. Rosenbluh, Absolute Raman cross-sections of some explosives: trend to UV, Opt. Mater. (Amst) 30 (2008) 1747–1754, https://doi.org/10.1016/j.optmat.2007.11.019.
[37] S. Almaviva, A. Palucci, S. Botti, A. Puiu, A. Rufoloni, Validation of a miniaturized spectrometer for trace detection of explosives by surface-enhanced Raman spectroscopy, Challenges 7 (2016) 14, https://doi.org/10.3390/challe7020014.
[38] Y. Liu, R. Perkins, Y. Liu, N. Tzeng, Normal mode and experimental analysis of TNT Raman spectrum, J. Mol. Struct. 1133 (2017) 217–225, https://doi.org/10.1016/j.molstruc.-2016.12.015.
[39] A.C. Ferrari, J. Robertson, Resonant Raman spectroscopy of disordered, amorphous, and diamondlike carbon, Phys. Rev. B. 64 (2001) 75414, https://doi.org/10.1103/PhysRevB.-64.075414.
[40] K. Nagashima, M. Nara, J.I. Matsuda, Raman spectroscopic study of diamond and graphite in ureilites and the origin of diamonds, Meteorit. Planet. Sci. 47 (2012) 1728–1737, https://doi.org/10.1111/maps.12007.